**Partially and fully de-alloyed glassy ribbons based on Au: Application in methanol electro-oxidation studies**

**Partially and fully de-alloyed glassy ribbons based on Au: application in methanol electro-oxidation studies**

Eirini Maria Paschalidou[1]*, Federico Scaglione[1], Annett Gebert[2], Steffen Oswald[2], Paola Rizzi[1], Livio Battezzati[1]

[1]Dipartimento di Chimica e Centro Interdipartimentale NIS (Nanostructured Surfaces and Interfaces), Università di Torino, Via Pietro Giuria 7, 10125 Torino, Italy

[2]Leibniz Institut für Festkörper- und Werkstoffforschung IFW, Helmholtzstraße 20, 01069, Dresden, Germany

*Corresponding Author: epaschal@unito.it

**Abstract**

In this work, electrochemical de-alloying of an amorphous alloy, $Au_{40}Cu_{28}Ag_7Pd_5Si_{20}$, cast in ribbon form by melt spinning, has been performed, obtaining self standing nanoporous materials suitable for use as electrodes for electrocatalytic applications. The de-alloying encompasses removal of less noble elements and the crystallization of Au, resulting in interconnected ligaments whose size and morphology are described as a function of time. Depending on de-alloying time, the crystals may contain residual amounts of Cu, Ag and Pd, as shown by Auger Electron Spectroscopy (AES), Energy Dispersive Spectroscopy (EDS) and Cyclic Voltammetry (CV) in a basic solution.

Current density peaks in the 0.16-0.28 V range (vs Ag/AgCl) indicate that the porous ribbons are active for the electro-oxidation of methanol. The partially de-alloyed samples, which still partially contain the amorphous phase because of the shorter etching times, have finer ligaments and display peaks at lower potential. However, the current density decreases rapidly during repeated potential scans. This is attributed to the obstruction of Au sites, mainly by the Cu oxides formed during the scans. The fully de-alloyed ribbons display current peaks at about 0.20 V and remain active for hundreds of scans at more than 60% of the initial current density. They can be fully re-activated to achieve the same performance levels after a brief immersion in nitric acid. The good activity is due to trapped Ag and Pd atoms in combination with ligament morphology.

**1. Introduction**

Nanoporous materials based on Au (NPG) have seen much progress due to the their potential applications as biosensors [1], substrates for enhanced Raman Spectroscopy [2], and catalysts for oxidation of alcohols [3-10], sugars [9], oxidation of CO [3,8,9,11], as for Oxygen reduction reaction [9]. They are most often

produced by de-alloying precursor alloys using chemical or electrochemical means [5,14,15]. In these processes, the less noble elements contained in the alloy are dissolved selectively, while the more noble ones assemble in open scaffolds of ligaments of nanometer size with pores in between, providing large accessible surfaces. These features, combined with their good electrical conductivity [16], make them suitable electrodes for electrocatalysis experiments [8,14].

Electrocatalysis of methanol oxidation is related to the technology of direct fuel cells (DMFC). Although Pt electrodes [12] show better electrocatalytic activity than Au, especially in an acidic environment, Au electrodes inhibit the formation of intermediates, which poison the catalytic sites for further reactions [7,10,17]. A drawback of porous Au is its tendency for coarsening, with a consequent reduction in activity. By adding small amounts of doping elements, e.g. Pd, it is possible to improve the stability of nanopores and the electrocatalytic performance [7]. Methanol electro-oxidation has been studied extensively in the literature [3-10], and therefore it constitutes a model reaction for estimating the efficiency and the stability of a catalyst, providing indications for the improvement of the catalytic material.

De-alloying is usually performed using binary *fcc* Au-Ag or Au-Cu random solid solutions having coarse grains. The removal of Ag or Cu induces the formation of channels in the grains by percolation and is accompanied by enhanced diffusion of Au atoms on the newly formed surface [14]. A network of ligaments builds up in each grain, which remains a single crystal after de-alloying [18]. Due to the fast surface diffusion which occurs during etching, it has been found that amounts of less noble atoms are trapped as impurities in the newly formed crystals [7].

Amorphous alloys are usually multicomponent materials frozen in the glassy state by rapidly quenching their melt. A complex composition is a requirement for glass forming ability, which is generally best at, or in the vicinity of, a deep eutectic point. The relative stability of these melts is due to the negative enthalpy of mixing between the alloy components, implying the occurrence of a short range order in the liquid which is retained in the glass [19,20]. The Au-based glass-formers are metal-metalloid systems in which preferential interactions occur between the metalloid Si and the metal atoms. The best ones in terms of quenching ability contain Au, Ag, Cu, and Pd in various proportions, summing up to about 80 % at. and 20 % at. Si [21].

The removal of less noble elements from the amorphous alloy shifts the composition outside the glass forming range, therefore de-alloying causes the formation of crystals rich in the noble components of the alloy. The noble atoms, freed from their neighbors, diffuse fast and cluster into numerous fine crystals at random in a large number of places; the crystals subsequently grow and impinge on each other, resulting in a network of ligaments separated by pores [1,22,23]. While the ligaments obtained from crystalline alloys are smooth and roundish, ligaments originated from amorphous precursors display grooved surfaces. It is then of interest to explore the effect of ligaments morphology on the properties of NPG [24].

Since the alloy is multi-component, it is expected that some less noble elements are incorporated in the new crystals, which can be of relevance in catalytic applications. In this work, we study in detail the progressive de-alloying of an amorphous alloy, $Au_{40}Cu_{28}Ag_7Pd_5Si_{20}$, as a function of time, extending previous findings on alloys of this family [7] and verifying the presence of impurity elements in ligaments by means of AES experiments in both partially and completely de-alloyed ribbons. The samples, having varied microstructure and composition, are then checked for their electro-catalytic ability to the electro-oxidation of methanol, this reveals the role of residual elements, namely Cu, Ag and Pd for the partially de-alloyed samples and Ag, Pd for the fully de-alloyed, in comparison with NPGs obtained via different routes.

**2. Experimental**

A $Au_{40}Cu_{28}Ag_7Pd_5Si_{20}$ master alloy [25] was fabricated by arc melting the pure elements (Au: 99.99%, Ag, Cu, Pd: 99.99%, Si: 99.99%) in an Ar atmosphere. Ribbons were produced by using melt spinning, i.e. ejecting the induction molten alloy through the nozzle of a silica crucible, onto a Cu wheel rotating at 20m/sin in an evacuated chamber and kept under an Ar pressure of ~ 1bar, while the overpressure applied to the alloy melt was 0.3 bar. The ribbon has a silvery color, is about 25 µm in thickness and 1.5mm wide. The surface, which was in contact with the wheel replicates its roughness and is dull, whereas the external surface has a shiny luster. The ribbon was cut to produce samples of 15mm in length.

A Potentiostat/ Galvanostat Model 7050 by Amel Instruments was used in a typical three electrode configuration. The electrochemical cell contained 1M $HNO_3$ aqueous solution, prepared using de-ionized water. For every de-alloying experiment, a new sample was used as a working electrode. Samples were de-alloyed for 5min, 10 min, 15 min, 30 min and for 1 hour, 3, 6 and 8 hours, by applying a potential of 1.05V vs Ag/AgCl [15], whose current density for dissolution reached values in the order of 1 $mA/cm^2$. The de-alloying procedure was made at 70°C, in order to have a suitable rate of etching [15]. In fact, amorphous alloys are known to be resistant to corrosion due to their homogeneous structure and lack of crystal defects such as grain boundaries.

A solution of 0.5M KOH and 5M $CH_3OH$ was used as an electrolyte for testing the electrocatalytic activity and the stability of the current density of the de-alloyed samples at room temperature. Before testing the working electrodes were activated for 1h in concentrated $HNO_3$ (69%), rinsed in de-ionized water for 15 min [15] and scanned for up to 20 cycles until the electrode is stabilized at a sweeping rate of 20 mV/s. Potentiodynamic scans were performed for 500cycles for all the samples. The samples de-alloyed for 6 and 8 h were reactivated after the 500 cycles experiment by immersion in concentrated $HNO_3$ for 20 min. The scans were repeated for another 500 cycles with the same sweeping rate. Before performing these experiments, the active electrochemical surface area was calculated for every working electrode by

performing CV scans in 0.5M KOH with a sweeping rate of 20mV/s. All current densities have been normalized by making use of the electrochemical active surface area of the electrode [4].

The surface morphology of de-alloyed samples was observed using Scanning Electron Microscopy (SEM) before and after electrocatalysis experiments and their composition was checked by Energy Dispersive X-ray Spectroscopy (EDS). The structure of the materials was studied using X-ray Diffraction (XRD) in Bragg-Brentano geometry with monochromatic Cu $K_{\alpha}$radiation, as well as High Resolution Transmission Electron Microscopy (TEM).

Auger Electron Spectroscopy (AES) measurements were made with a JEOL JAMP 9500F Scanning Auger Microprobe which had a hemispherical analyzer, a chamber pressure of $10^{-7}$Pa (without sputtering) and a Schottky field emission source. The analyzer was operated setting the constant retarding ratio (CRR) mode at 0.32, resulting in a relative energy resolution of 0.5%. The electron beam conditions were at 10keV and 10nA. Direct spectra were used for evidencing the presence of elements and differential spectra for concentration calculations. Data manipulation was made by means of the PHI-MULTIPAK software [36]. The ribbons were sputtered with 2keV $Ar^{+}$ ions with a sputtering rate of 17 nm/min, to remove any possible surface contamination occurring after fracture of the samples in air. The chemical analysis was performed on the cross section of fractured samples by scanning over several spots in neighboring zones, starting from the outside and then moving towards the inside part.

## 3. Results and Discussion

### 3.1 The process of de-alloying

Full de-alloying of a 25µm thick ribbon requires 6 h of polarization at 1.05V vs Ag/AgCl at 70 °C. The slow etching allows the avoidance of cracking the alloy due to stress corrosion and rapid volume reduction [14]. Three time steps are evidenced: in the initial transient time the current density increases progressively to the desired value, while passive layers on top of the ribbon are removed and percolation channels are formed inside the material. In the second step, the current density remains approximately constant for hours during which the bulk of the ribbon is etched. In the last period, the residual thicker parts of the ribbon are de-alloyed and the current density shows a downward trend, falling finally to a steady background level when the process is complete [15].

The size of the ligaments made of the fine crystals originating from the amorphous phase increases up to a value which was found to depend on the temperature of the solution [15] (results reported here refer only to 70 °C) and then remains substantially constant. This is apparent in Fig. 1, which shows images of ribbon portions after various de-alloying times. The development of the porous structure occurs on both surfaces of the ribbon, with the appearance of channels and irregular rafts, which evolve progressively into pores

and ligaments through the thickness, without apparent differences between the air side and the wheel-side, or inside the bulk. The thickness of the porous layer increases steadily via movement of a sharp interface, well apparent in the cross sections in Fig. 1(g-i), indicating that the electrolyte penetrates into the pores without obstacles. The completion of the process occurs in different times along the ribbon because its thickness varies locally. After 6 h, the ribbon is fully de-alloyed and the two interfaces join together, becoming a single dividing surface, which is weaker than the rest of the ribbon and therefore fractures more easily. However, the integrity of the ribbon is maintained in the absence of stress, e. g. the shear stress applied by cutting to obtain the cross section. Ligaments and pores form in the early stages and reach an average size [15] already during the shortest measuring period of 5 min of processing (Fig. 1(j)) because of coarsening due to supply of atoms by diffusion at an appropriate distance, afterwards they remain roughly constant for long time periods. This confirms previous reports [22], which showed that the coarsening of ligaments follows a kinetics similar to that of de-roughening of Au electrodes in contact with aqueous solutions, a typical surface diffusion process [26].

### 3.2 Characterization of partially and fully de-alloyed samples

#### 3.2.1 Structure, morphology and composition of ligaments

XRD patterns of samples de-alloyed for increasing amounts of time reveal that the intensity of the amorphous halo lowers and that reflections due to a *fcc* crystalline phase with random orientation develop, with a lattice constant always close to that of Au (Fig. S1 in Supplementary Information). The amorphous halo is still recognizable after 1 h of de-alloying since the X-rays penetrate through the pores, whereas Differential Scanning Calorimetry (DSC) scans reveal that the crystallization of the remaining glassy phase occurs for processing up to at least 4 h [15]. The envisaged presence of small quantities of Ag and Pd dissolved in Au cannot be detected in XRD patterns, since the lattice constant of their diluted solutions differs only slightly with respect to that of the Au element [29]. The fact that there is no appreciable decrease in lattice spacing, which would be expected if the Au alloy contained a substantial amount of Cu, indicates that the Cu detected by AES and EDS (see below) is confined in the surface layers and is possibly in an oxidized state. The reflections of the *fcc* phase are rather broad, indicating the material contains fine scattering domains, whose size was estimated to be a few tens of nanometers according to Rietveld analyses of patterns. Actually, the ligaments are made of multiple crystals which were originated independently from each other. The TEM image reported in Fig. 2 shows a ribbon mechanically thinned to transparency before undergoing almost complete de-alloying. It represents a snapshot of the early stage of formation of pores and crystals whose lattice fringes extend for a few nanometers in different directions. When an entire ribbon is de-alloyed, the crystals grow and impinge forming boundaries, which are

indicated by grooves on the external surface of the ligaments (see Fig. 1(f)). This morphology is at variance to that encountered in de-alloying crystalline solid solutions when much smoother ligaments and roundish pores are obtained [14,16].

The SEM-EDS analysis of both sides of the as-spun ribbon confirms it is homogeneous, in accordance with the nominal composition. After de-alloying for 15 min, crystalline protrusions are already well developed, but the amorphous part is still exposed; therefore EDS not only reveals the predominance of Au, but also substantial quantities of the other elements: e. g. the Si content, which is measured at 6 at.-% and must originate from the underlying glassy phase, considering that the crystallization of Au implies that all Si is removed from the uppermost layers. At variance, the comparatively high amount of 19 at.% found for Cu must be due to contributions of both crystalline and amorphous zones. The content of Ag and Pd of 2.8 at.% and 1.1 at.%, respectively, must be due to both contributions as well. These are average values resulting from several measurements on different parts of the surface and are affected by a scatter in the order of 30%. It is therefore concluded that the Cu, Ag and Pd remain trapped to some extent in the protrusions and ligaments although their local content cannot be determined precisely. In the sample de-alloyed for 30 min, the Si, Ag and Pd are detected only at places, while Cu is still found at a level of 7 at.%. Preliminary X-ray Photoelectron Spectroscopy (XPS) results indicate that Cu occurs in the uppermost layers of the surface as monovalent oxide, whereas a few nanometers below the surface all elements are metallic. After de-alloying for longer times, mostly Au is detected in the ligaments by performing EDS at various positions; however, inspection of spectra clearly revealed local traces of Pd and Ag, although their amount cannot be quantified. AES was performed at various points on the cross section of the nanoporous part of the samples after two minutes of sputtering (Fig. S2a and S2b in Supplementary Information). The regions of direct spectra relevant for the elements of interest here are shown in Fig. 4 for the samples de-alloyed for 30 min (Fig. 3(a-c)) and for 6 h (Fig. 3(d-f)). They are representative of the results for short and long de-alloying times, respectively. The direct spectra for both samples indicate that no Si is still present in the nanoporous part of the ribbon and Cu is detected only in the sample de-alloyed for 30min. Quantitative data are obtained using the peak to peak heights in the differentiated AES spectra (not reported) [36]. The Cu concentration after 30 min of de-alloying is around 2.2 at.%, whereas in the sample de-alloyed for 6 h, it falls below the detection limit. On the other hand, Pd and Ag are revealed at all times in direct spectra and are also found in detectable amounts of 0.5-0.7 at.% in differential ones, for the sample de-alloyed for 6 h. It is then concluded that trapping of some minority components occurs as in the case of de-alloying crystalline alloys, e. g. Pt in ternary Au-Ag-Pt [28]. However, it is stressed that the combination of surface kinks due to grain boundaries and residual elements occurs only in the case of de-alloying of an amorphous alloy. This might influence the distribution of solutes in the Au crystals because of segregation.

### 3.2.2 Electrochemical behaviour of de-alloyed materials in basic solution

Cyclic voltammetry (CV) scans in 0.5 M KOH of the nanoporous electrodes, suggest the occurrence of various processes on the surface of the samples, due to their microstructure and local composition. Results are shown in Fig. 4. During the positive scan, chemisorption of $OH^-$ ions on the electrodes occur in the non-faradaic potential range, leading to the formation of Au oxides [5,7], which are marked by the current peak at around 0.22V. The increased current intensity is due to the varying thickness of the porous layer.

The literature indicates that the potential range where the formation of oxides of nanoporous Au takes place is close to that for the formation of AgO, dependent on the operational conditions (pH value, number of cycles, scan speed, concentration of the electrolyte) [29,31]. This was confirmed in the present case by making cyclic voltammetry experiments in KOH with an Ag electrode in the expanded potential range from -0.5 V to 0.7 V vs Ag/AgCl: the formation of $Ag_2O$ and AgO has been found to correspond to current peaks at around 0.30 V and 0.55V (vs Ag/AgCl) on the forward scan, while their reduction was observed at 0.25 V and -0.04 V in the backward scan, respectively. With this evidence, the low intensity signals obtained for some samples above 0.3 V (Fig. 4) are attributed to the presence of some residuals Ag on the surface. A further small peak is reproducibly found at about 0.06V for the samples de-alloyed for 3,6 and 8 h (Fig. 4), which is attributed to the oxidation of the trapped Pd atoms remaining in the ligaments [30-32].

During the negative scan Au oxides are reduced, giving the corresponding peak. The position of the reduction peak is known to depend both on the ligament size and on surface composition [5]. In our experiments, the broad signal must be a result of multiple overlapping processes, due to the complex surface chemistry of the samples involving the reduction of different species.

### 3.3 Methanol electro-oxidation on partially and fully de-alloyed porous Au electrodes.

The partially and fully de-alloyed Au electrodes are electrocatalytically active for methanol oxidation in basic solutions, as shown by repeated CV cycles in 0.5 M KOH + 5 M $CH_3OH$. The first cycles for each of the electrodes show current density peaks reaching values in the order of milliAmperes per square centimeters (Fig. 5); this is comparable with the highest ones reported in the literature in the case of NPG films made by means of a complex procedure of alloying/de-alloying smooth electrodes [33]. For the samples which were de-alloyed for 15 and 30 min and which have finer ligaments, both the onset of the oxidation reaction and the maximum of the current peak occur at lower potentials compared to those of the other samples. Furthermore, the values of the current density are higher for these two samples.

It was earlier established that the methanol electro-oxidation on NPG occurs in two ranges of potential giving two current peaks [5,10,16]: at lower potentials, from -0.1V to 0.35V vs Ag/AgCl, methanol is oxidized to formate ions with the exchange of 4 electrons according to the reaction:

$$CH_3OH+5OH^-=HCOO^-+4H_2O+4e^- \quad (1)$$

Meanwhile, at potentials above 0.4V, methanol is oxidized to carbonates with the exchange of 6 electrons according to the reaction:

$$CH_3OH+8OH^-=CO_3^{-2}+6H_2O+6e^- \quad (2)$$

During the positive scan and at the onset of the current peak, $OH^-$ ions are chemisorbed on the electrode and pre-oxidized species such as Au-OH(1-λ)$^-$ form, where λ is the charge transfer coefficient. The anodic current then displays a neat peak due to reaction (1). The consumption of the Au-OH(1-λ)$^-$ species on the electrode for the formation of Au-oxides leads to a drop in the current for methanol oxidation [5,16,17]. When more positive potentials are reached, there is reactivation of the anodic oxidation of methanol on Au oxides and so the current increases again (reaction (2)).

Therefore, the current peaks seen in Fig. 5, with maxima occurring between 0.16 V and 0.28 V are due to oxidation according to reaction (1).

As the potential sweeps negatively, in the same potential range where Au oxides are reduced (from 0.17V to -0.06V), the oxidation of methanol is resumed according to reaction (1) and a current peak appears again.

On increasing the potential above 0.35 V, the samples de-alloyed for shorter amounts of time give a steep increase in current density as a result of methanol electro-oxidation, not only on Au oxides but also on Cu oxides [34]. This is demonstrated by a decrease in intensity of the oxidation current with increasing de-alloying time, i. e. with less Cu available on the surface of samples. It was also proven by performing scans with pure Cu and with as-cast ribbons as working electrodes, which provided current peaks in the potential region expected for the reaction on Cu oxides [34] (Figs. S3 and S4 in Supplementary Information).

Figs. 6 (a) and (b) show CV scans selected out of those recorded during 500 cycles of electro-oxidation of methanol, using the samples de-alloyed for 30 min and 6 h, respectively. These scans are representative of the behavior of either partially de-alloyed electrodes which expose to the solution varied amounts of ligaments as well as the residual amorphous phase, or fully de-alloyed electrodes which consist of ligaments and pores only.

Due to the complexity of these electrodes, both in composition and in microstructure, it is believed that the anodic current peaks result from various contributions. Because of the different de-alloying times, the amount of each element differs from sample to sample. In the potential range from -0.1V to 0.35V vs Ag/AgCl, the sample which is de-alloyed for 5 min gives lower current density with respect to the other electrodes, due to the still thin de-alloyed nanoporous part (Fig. 1j). By increasing the de-alloying time, the de-alloyed volume increases, providing higher current density with respect to the previous sample. In the case of short de-alloying times (10 min or less), the amount of less noble elements which remain entrapped in the fine ligaments, along with the remaining amorphous phase, provide several contributions to the current density, such as the formation of Cu, Ag and Pd oxides [29,30,34,35,37,38]. These contributions

cause apparent shifts in the potential corresponding to the maximum of the current density. The lower value of the potential occurs when the ligaments' morphology has reached a steady state, at a distance from the amorphous-ligament interface and after 15 min of de-alloying. As detailed above, Cu is detected especially in the samples de-alloyed for short time periods, whereas mostly Au with traces of Ag and Pd occur during the later stages of processing. This, together with the limited size of the Au rich ligaments, affects the intrinsic catalytic activity of electrodes. During the early cycles with the samples de-alloyed for short time periods, both methanol electro-oxidation on Au(Pd) [7] and the formation of Cu and Ag oxides [33-35] contribute to the current density in the low potential region (≤ 0.35 V). After repeating CV scans, the electrodes become covered with Cu and Ag and Pd oxides [29,30,31,34,35,37,38], which diminish the number of exposed active Au sites causing a substantial drop of the current density after a limited number of cycles for both reactions (1) and (2). When the Cu is fully dissolved, i.e. for long de-alloying times, the electrodes are less inhibited since reaction (2) occurs at a higher potential on Au; therefore they remain active for reaction (1), with a limited drop of current during cycling. In the high potential region (>0.35 V), the current density provided by samples de-alloyed for short time periods increases in the first tens of cycles and then decreases. This fact confirms methanol oxidation on Cu oxides, as well as that after the continuous cycling of the sample and the dissolution of the Cu, the methanol oxidation occurs only on Au oxides via reaction (2).

In the negative scan, from 0.3V to -0.1 V, the current density increases due to methanol electro-oxidation on Au atoms which are produced by the reduction of Au oxides (0.2V and lower) according to reaction (1) [5,10]. Especially for the samples that are de-alloyed short time periods, it seems that there are several contributions to the current density, taking into account that in this potential range the reduction of Ag oxides takes place as well [29,31].

To show the electrochemical stability of each electrode, the current density at the maximum of the CV scan is plotted in Fig. 6(d) as a function of the number of cycles, normalized with respect to the maximum value recorded in the first cycle [7]. Although the reactions are initially more favored for the samples de-alloyed for 15 and 30 min in terms of potential, these have limited stability, since after 500 cycles the current density drops to a small percentage of the initial value. On the other hand, the samples de-alloyed for 6 and 8 h (fully de-alloyed) display very good stability after 500 cycles, showing efficiency up to 60% and 50%, respectively. These results are comparable with others appearing in the literature [7], although the ligament size of our samples (~200 nm) is four times larger. For a closer comparison a porous electrode was produced in this work by de-alloying a crystalline alloy, $Au_{31}Cu_{41}Zn_{12.8}Mn_{15.2}$, which does not contain Ag and Pd, obtaining ligament size in the same range as those of the electrodes made with the present amorphous alloy [24]. The current density for methanol oxidation via reaction (1) was lower and the intensity of the current peak decreased to zero in a few cycles, clearly demonstrating the contribution of

the trapped atoms of Ag and Pd as well as that of the necks present in the ligaments; the latter provide surface kinks which may play a positive role in the electrocatalytic activity. Also, the amorphous layer, which is not yet de-alloyed in the early stage of the process, has a significant influence, though adverse, on the electrochemical performance of the electrodes, since it is a source of less noble elements, especially Cu. The study of electro-catalytic activity as a function of progressive de-alloying reveals the role of various elements: the Au:Cu:Ag:Pd ratio in the present alloy (40:28:7:5) differs with respect to that (30:33:7:10) of a previous report in which Ag was not apparently detected [7]. This might suggest an effect of composition of the starting material on the amount of trapped atoms which, however, is not proven since residual Ag and Pd were both found in a de-alloyed $Au_{30}Cu_{38}Ag_7Pd_5Si_{20}$ metallic glass [2].

After 500 cycles the re-activation of the electrodes de-alloyed for 6 and 8 h was attempted by immersing them again in $HNO_3$ for 15 min. Having verified with CV scans in 0.5M KOH that the effective surface area did not change appreciably, the electro-catalysis experiments were repeated for another 500 cycles under the same conditions as previously. The results are shown in Fig.6(c). For the sample de-alloyed for 6 h, the value of the current density for the first cycle has exactly the same value (0.68mA/cm$^2$) as in the first experiment, with a small shift of the value of the potential, which is 0.02V more positive than the previous one. For the 8 h sample, the current density is 0.59mA/cm$^2$ instead of 0.79mA/cm$^2$ (Fig. S5 in Supplementary Information) and the value of the potential is close to the previous one, namely 0.28V. The current stability after the second set of 500 cycles is again comparable, reaching 60% and 52%, respectively, for the sample de-alloyed for 6 h. These results indicate that the ribbon is more stable in its fully de-alloyed state, while its performance is decreased when it is etched for very long periods, probably because of the loss of Ag and Pd atoms.

**4. Conclusions**

In this work, free standing porous ribbons suitable for application as electrodes have been obtained by de-alloying of an amorphous alloy, $Au_{40}Cu_{28}Ag_7Pd_5Si_{20}$. The progression of the etching process has been followed showing that fine Au-based crystals form, grow and impinge on each other developing a continuous network of ligaments separated by pores. The ligaments are constituted by several crystals of tens of nanometer size [23], randomly oriented and separated by grain boundaries, which cause grooving of the surface, contrary to NPG produced by de-alloying crystalline alloys [24]. Since amorphous alloys are inherently resistant to corrosion, lacking grain boundaries and other crystal defects, the de-alloying must be made at a temperature, in order to progress in a reasonable time period of a few hours. This causes coarsening of ligaments to around 200 nm. On the other hand, the relatively slow development of ligaments helps in keeping the integrity of the ribbon by relaxing local stresses and volume reduction.

Electrochemical evidence indicates that amounts of Ag and Pd are trapped locally in the crystals. Both these features appear essential for the good electrocatalytic behaviour of the ribbons.

Both partially and fully de-alloyed ribbons are active in catalyzing methanol electro-oxidation in a basic solution to either forming formate ions in the potential range of 0.16-0.28 V, or carbonate ions at higher potential (> 0.35 V). Partially de-alloyed materials display current peaks at lower potential, but still contain a substantial quantity of Cu in the amorphous matrix, which is oxidized during the potential sweeps. Cu oxides are active for methanol electro-oxidation at a high potential, but their presence inhibits the Au sites active in the low potential range. Therefore, the current density for methanol oxidation to formate ions decreases steadily when performing successive scans, becoming almost nil after less than five hundred cycles. Fully de-alloyed ribbons (obtained after 6 h of etching), on the other hand, remain active to more than 60% of the initial current density after five hundred cycles, without further apparent decay and can be re-activated by briefly immersion in nitric acid. It was found that the trapped Pd and Ag atoms contribute to methanol oxidation at low potential, favoring the persistence of a substantial current density on repeated scans of the potential. Etching for longer times decreases the electrode performance.

**Acknowledgements**

This work was supported by the funding scheme of the European Commission, Marie Curie Actions — Initial Training Networks (ITN) in the frame of the project VitriMetTech — Vitrified Metals Technologies and Applications in Devices and Chemistry, 607080 FP7-PEOPLE-2013-ITN.

**Figure Captions**

Fig. 1. SEM images of ribbon portions de-alloyed for 5min or more. Figs. (a-e) are the top views for the de-alloyed ribbons and Figs. (g-i) the cross section views. Image (f) shows an enlarged view of the sample de-alloyed for 6 h. The plot (j) shows the ligament size (left scale, squares) and de-alloyed thickness (right scale, blue circles) as a function of time. Red squares are for air side and black squares for wheel side of the ribbon. The bars refer to the left axis and represent $\pm$ one standard deviation with respect to the mean of the distribution of size values.

Fig. 2. TEM image for a sample de-alloyed for 30sec. The early stage formation of pores and crystals whose lattice fringes extend for a few nanometers in different directions.

Fig. 3. Part of AES direct spectra referring to the minority elements of the amorphous alloy de-alloyed for 30 min: Pd, Ag, Cu, Si (a-c) and for the sample de-alloyed for 6 h: Pd, Ag, Cu, Si (d-f).

Fig. 4. CV scans in the potential range from -0.1 to 0.5 vs Ag/AgCl in 0.5 M KOH of nanoporous electrodes that were produced at different de-alloying times.

Fig. 5. CV scans (first cycle) performed in 0.5 M KOH + 5 M $CH_3OH$ with ribbons de-alloyed 15 min, 30min, 1 h, 3 h, 6 h, and 8 h showing the electro-oxidation of methanol.

Fig. 6. CV scans performed for 500 cycles at the scan rate of 20 mV/s in 0.5 M KOH + 5 M $CH_3OH$ using as working electrode the ribbon de-alloyed for 30 min (a), the ribbon de-alloyed for 6 h (b), the ribbon de-alloyed for 6 h after re-activation for the second group of 500 cycles (c). The maximum current density in selected CV scans normalized with respect to the maximum value which is recorded in the first scan as a function of the number of cycles for electrodes de-alloyed 30 min, 6 h and 8 h. Wine symbols: first group of 500 scans; blue symbols: second group of 500 scans made after re-activating the electrode (d).

**References**


[1] J. Yu, Y. Ding, C. Xu, A. Inoue, T. Sakurai, M. Chen, Chem. Mater., 20 (2008) 4548-4550

[2] F. Scaglione, E. M. Paschalidou, P. Rizzi, S. Bordiga, L. Battezzati, Phil. Mag. Lett. 95 (2015) 474–482

[3] A. Wittstock, J. Biener, M. Bäumer, Phys. Chem. Chem. Phys., 12(2010) 12919-12930.

[4] S. Xiao, F. Xiao, Y.Hu, S. Yuan, S. Wang, L. Qian, Y. Liu, Scientific Reports, 4(2014) 4370.

[5] J. Zhang, P. Liu, H. Ma, Y. Ding, J. Phys. Chem. C, 111 (2007) 10382-10388.

[6] K. A. Assiongbon, D. Roy, Surface Science, 594, (2005) 99-119.

[7] X. Y. Lang, H. Guo, L. Y. Chen, A. Kudo, J. S. Yu, W. Zhang, A. Inoue, M. W. Chen, J. Phys. Chem. C, 114 (2010) 2600-2603.

[8] H.-J. Qiu, H.-T.Xu, L. Liu, Y. Wang, Nanoscale, 7(2015) 386-400.

[9] P. Rodriguez, M. T. M. Kopper, Phys. Chem. Chem. Phys., 16, (2014) 13583-13594.

[10] Z. Borkowska, A. Tymosiak- Zielinska, G. Shul, Electrochim. Acta, 49 (2004) 1209-1220

[11] T. Fujita, P. Guan, K. McKenna, X. Lang, A. Hirata, L. Zhang, T. Tokunaga, S. Arai, Y. Yamamoto, N. Tanaka, Y. Ishikawa, N. Asao, Y. Yamamoto, J. Erlebacher, M. Chen, Nat. Mater. 11 (2012) 775-780

[12] X.Y. Lang, G.F. Han, B.B. Xiao, L.Gu, Z.Z. Yang, Zi. Wen, Y.F. Zhu, M. Zhao, J.C. Li, Q Jiang, Adv. Funct. Mater. 25 (2015) 230-237.

[13] X. Y. Lang, H. Y. Fu, C. Hou, G.F. Han, P. Yang, Y. B. Liu, Q. Jiang, Nat. Commun., 4 (2013) 2169-2176

[14] J. Weissmueller, R. C. Newman, H.-J. Jin, A. M. Hodge, J. W. Kysar, MRS Bulletin, 34 (2009) 557-586.

[15] F. Scaglione, P. Rizzi, L. Battezzati, J. Alloys Compd., 536S (2012) S60-S64.

[16] Y. Ding, M. W. Chen, MRS Bulletin,34 (2009) 569-576.

[17] B. Beden, J. M. Leger, C. Lamy, Electrocatalytic Oxidation of Oxygenated Aliphatic Organic Compounds at Noble Metal Electrodes in Modern Aspects of Electrochemistry, J.O'M. Bockris, B. E. Conway, R.E. White, Eds; Plenum Press: New York, Vol. 22, (1992) pp. 97-264.

[18] S. Van Petegem, S. Brandstetter, R. Maass, A. M. Hodge, B.S. El-Dasher, J. Biener, B. Schmitt, C.Borca, H. Van Swygenhoven, Nano Lett., 9 (2009) 1158-1163.

[19] L. Battezzati, Metallic Glasses in Chemical Thermodynamics, a Chemistry for the 21st Century monograph, T. M. Letcher Ed., Blackwell Science, Oxford, UK, 1999;pp. 239-249.

[20] M. Telford, Materials Today, 7 (2004) 36-43.

[21] J. Schroers, B. Lohwongwatana, W. L. Johnson, A. Peker, Appl. Phys. Lett., 87 (2005) 061912.

[22] P. Rizzi, F. Scaglione, L. Battezzati,J. Alloys Compd., 586 (2012) S117-S120 .

[23] F. Scaglione, P. Rizzi, F. Celegato, L. Battezzati,J. Alloys Compd., 615 (2014), S142-S147.

[24] F. Scaglione, F. Celegato, P. Rizzi, L. Battezzati, Intermetallics 66 (2015) 82-87]

[25]H. Guo, W. Zhang, C. Qin, J. Qian, M. Chen, A. Inoue, 50 (2009) 1290-1293

[26] J. M. Dona, J. Gonzalez Velasco, J. Phys. Chem., 97 (1993), 4714-4719.

[27] W. B. Pearson, A Handbook of Lattice Spacings and Structures of Metals and Alloys, Pergamon Press, Oxford, UK, (1958).

[28] A. A. Vega, R. C. Newman, J. Electrochem. Soc., 161 (2014) C1-C10.

[29] Y. Wan, X; Wang, S; Li, Y; Sun, H. Liu, Q. Wang, Int. J. Electrochem. Sc., 8 (2013) 12837-12850.

[30] Z. X. Liang, T. S. Zhao, J. B. Xu, L. D. Zhu, Electrochim. Acta, 54 (2009) 2203-2208.

[31] M. Grden, M. Lukaszewski, G. Jerkiewicz, A. Czerwinski, Electrochim. Acta, 53 (2008) 7583-7598.

[32] Y.-Y. Yang, J. Ren, H. -X. Zhang, Z.-Y. Zhou, S.-G. Sun, W. -B. Cai, Langmuir, 29 (2013) 1709-1716.

[33] C. Yu, F. Jia, Z. Ai, L.Zhang, Chem. Mater., 19 (2007) 6065-6067.

[34] H. Heli, M. Jafarian, M. G. Mahjani, F. Gobal, Electrochim. Acta, 49 (2004) 4999-5007.

[35] G. Orozco, M. C. Pérez, A. Rincòn, C. GutiérrezJ. Electroanal. Chem., 495 (2000), 71-78.

[36] MultiPak, software package, V. 9.3, ULVAC-PHI, 1994- 2011.

[37] S. S. Abd El Rehim, H. H. Hassan, M. A. M. Ibrahim, M. A. Amin, Monatsh Chem., 192 (1998) 1103-1117

[38] M. C. Jeong, C. H. Pyun, I.H. Yeo, J. Electrochem. Soc., 140 (1993) 1986-1989

[39] J. M. M. Droog, C. A. Alderliesten, P. T. Alderliesten, G. A. Boottsma , J. Electroanal. Chem., 111 (1980) 61-70

[40] Riyanto, M. R. Othman, J. Salimon, MJAS, 11, No2 (2007) 379-387

**Figure 1**

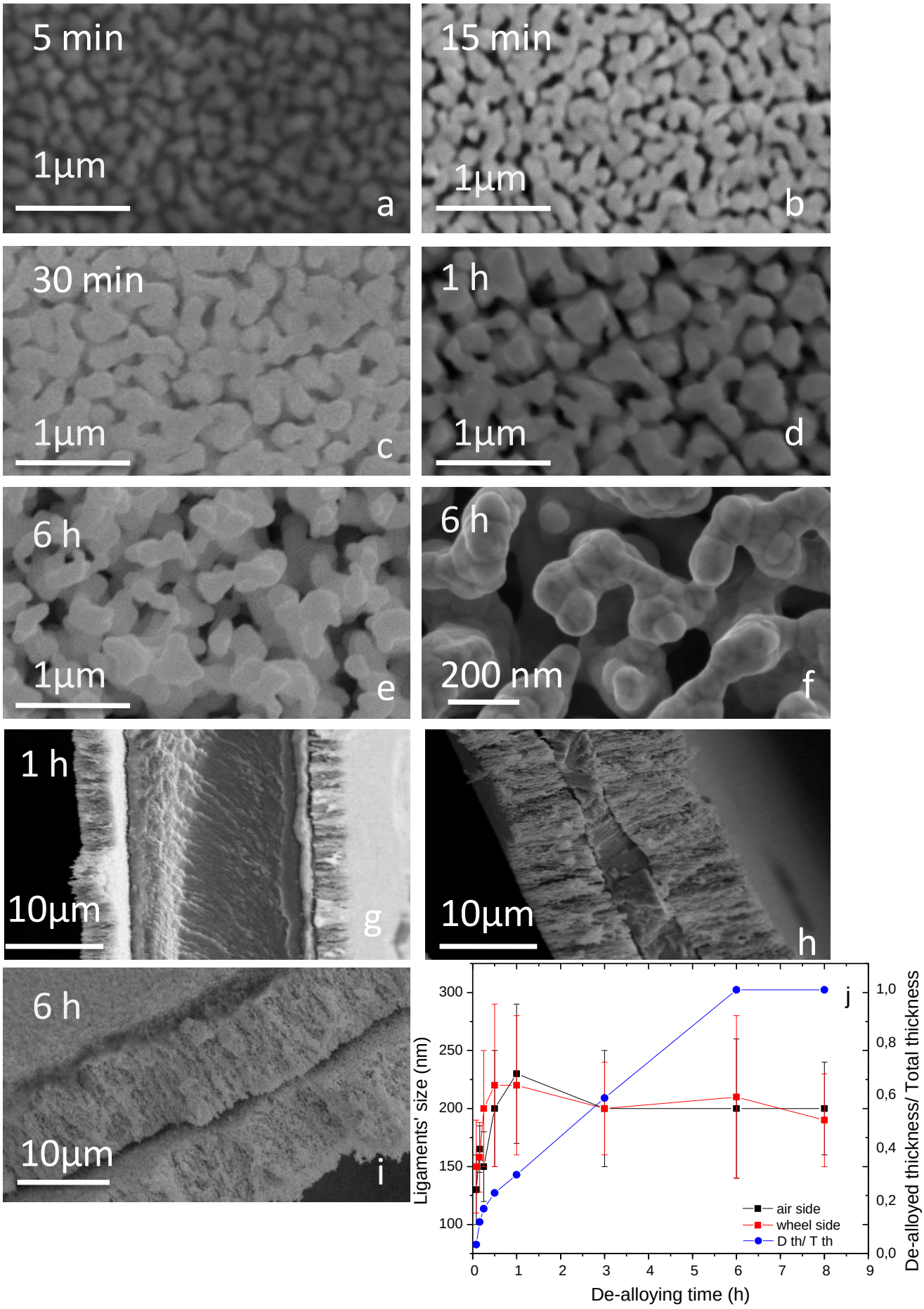
5 min
1µm
a
15 min
1µm
b
30 min
1µm
c
1 h
1µm
d
6 h
1µm
e
6 h
200 nm
f
1 h
10µm
g
10µm
h
6 h
10µm
i
j
Ligaments' size (nm)
De-alloyed thickness/ Total thickness
De-alloying time (h)
air side
wheel side
D th/ T th

**Figure 2**

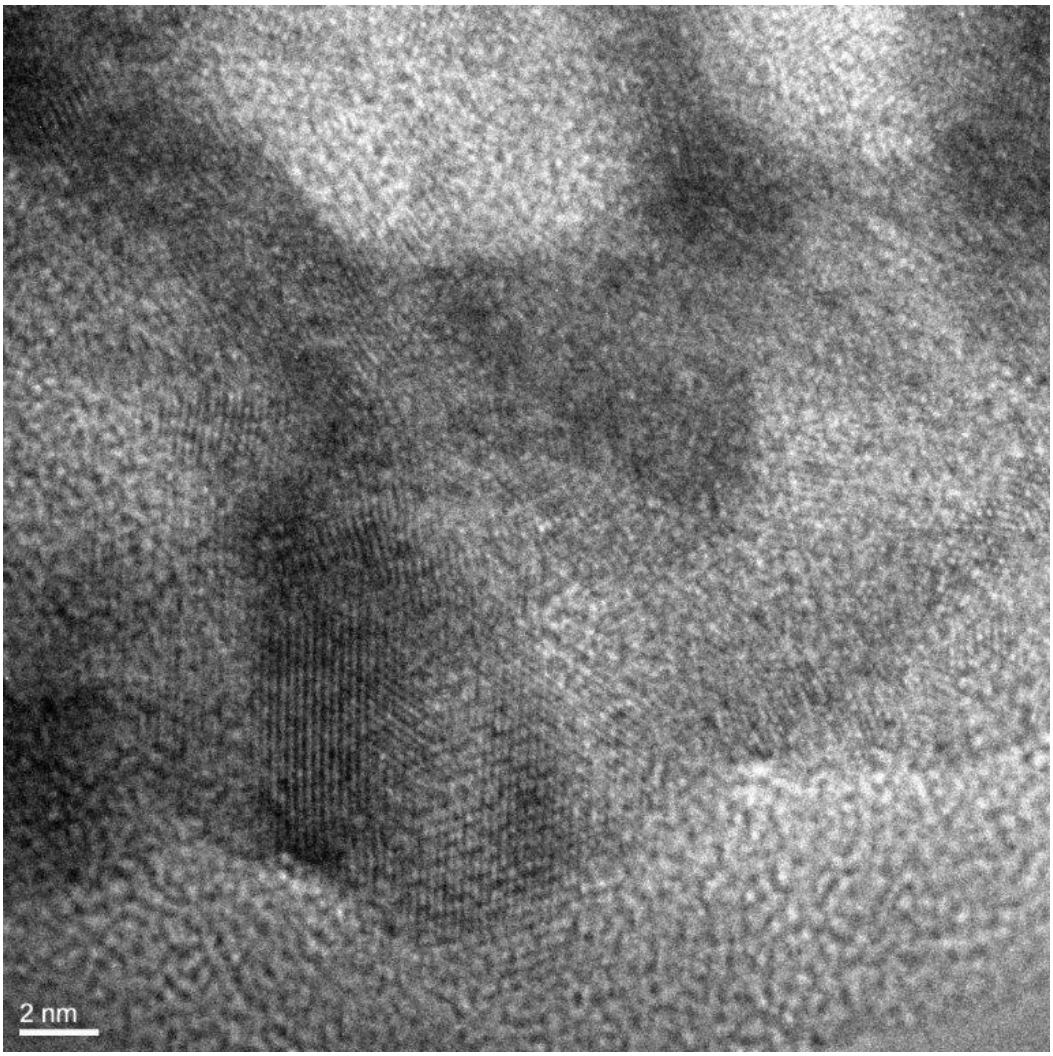

**Figure 3**

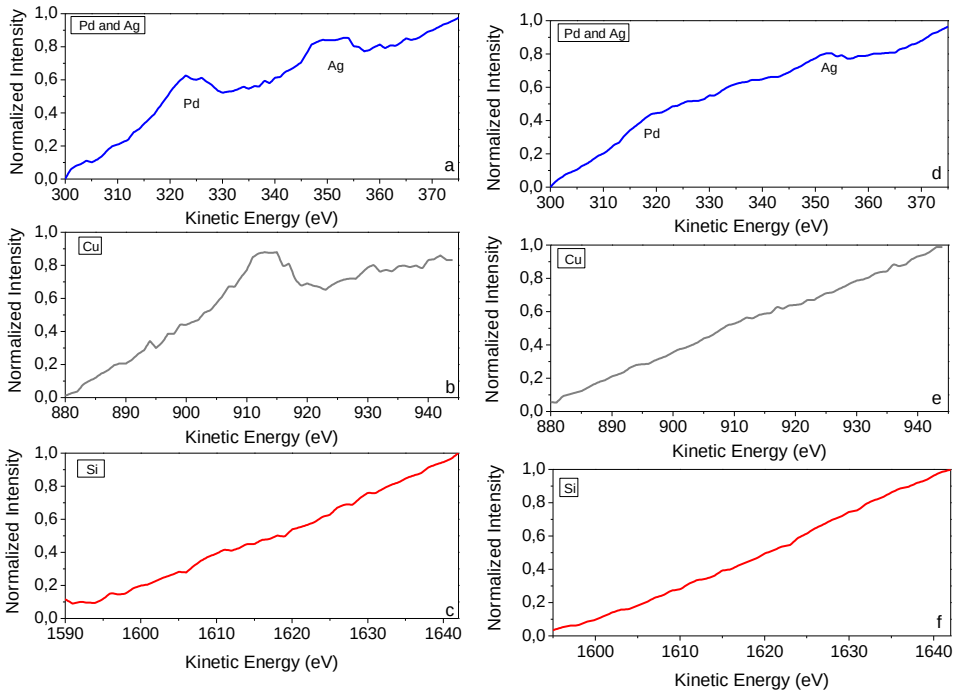
Pd and Ag
Pd
Ag
a
Normalized Intensity
Kinetic Energy (eV)
Cu
b
Si
c
d
e
f

**Figure 4**

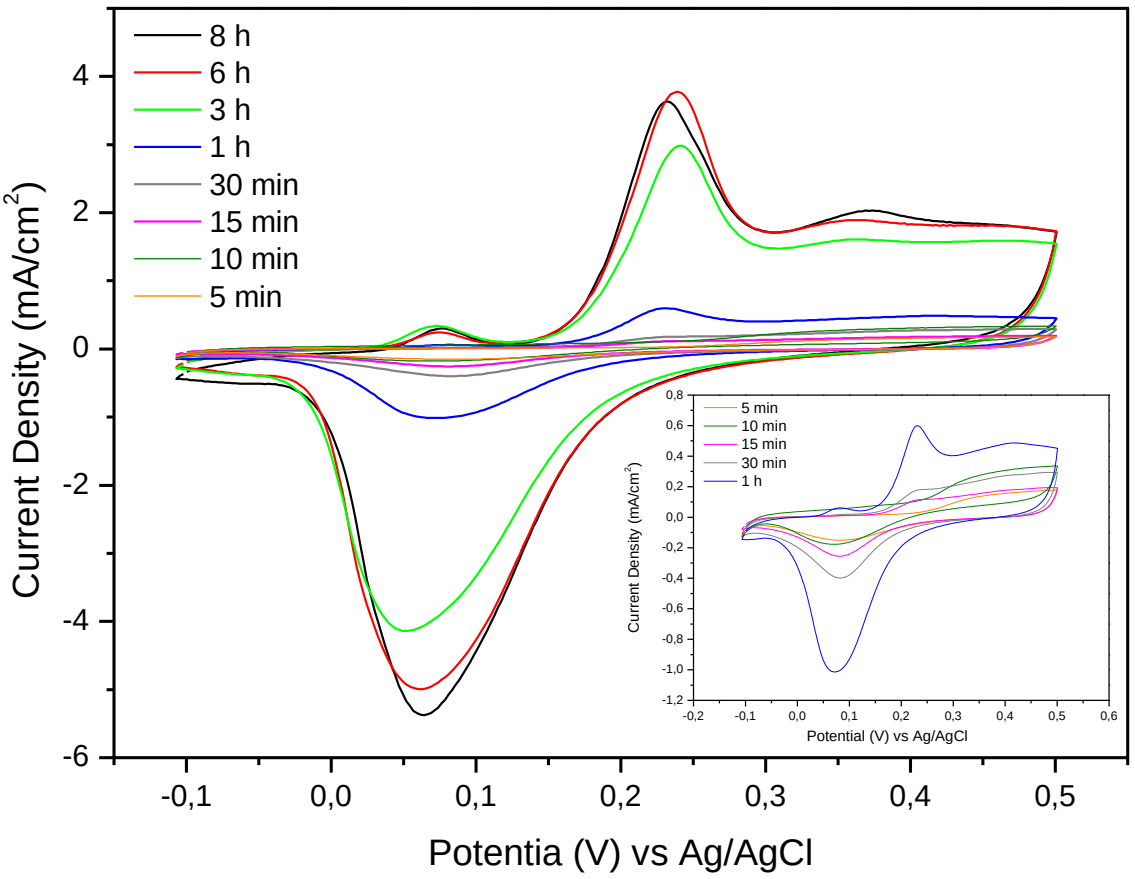
8 h
6 h
3 h
1 h
30 min
15 min
10 min
5 min
Current Density (mA/cm$^2$)
Potentia (V) vs Ag/AgCl
Current Density (mA/cm$^2$)
Potential (V) vs Ag/AgCl

**Figure 5**

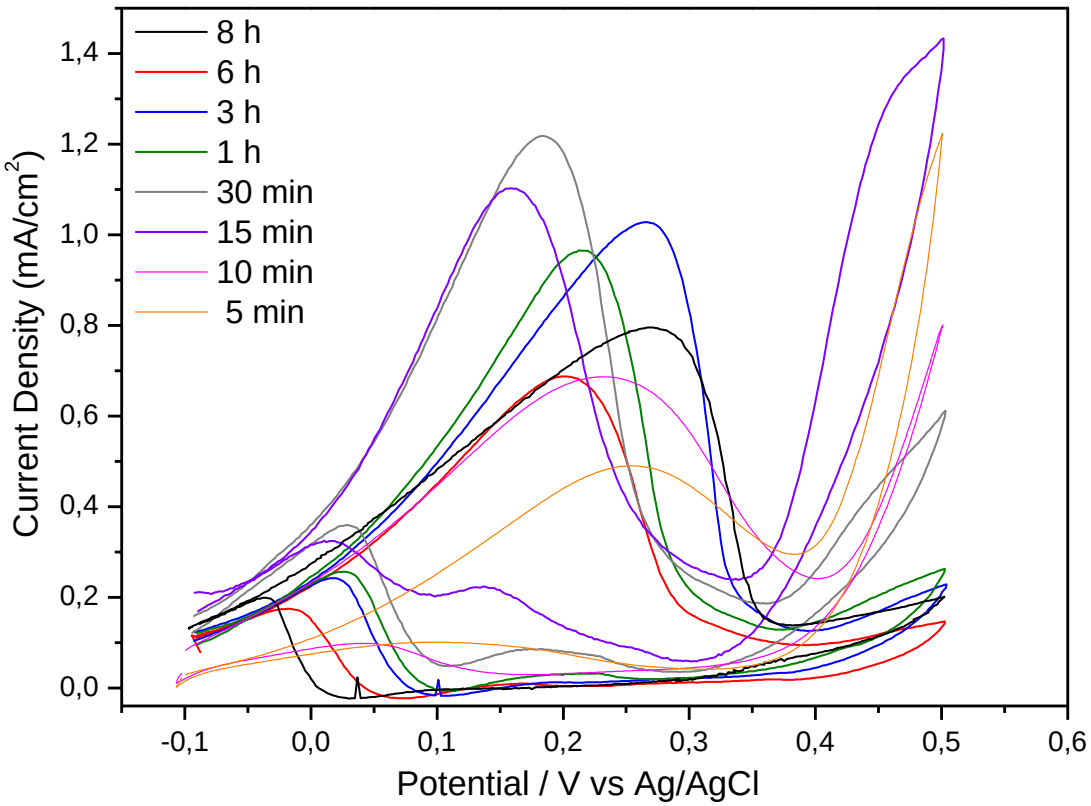
8 h
6 h
3 h
1 h
30 min
15 min
10 min
5 min
Current Density (mA/cm2)
1,4
1,2
1,0
0,8
0,6
0,4
0,2
0,0
-0,1
0,0
0,1
0,2
0,3
0,4
0,5
0,6
Potential / V vs Ag/AgCl

**Figure 6**

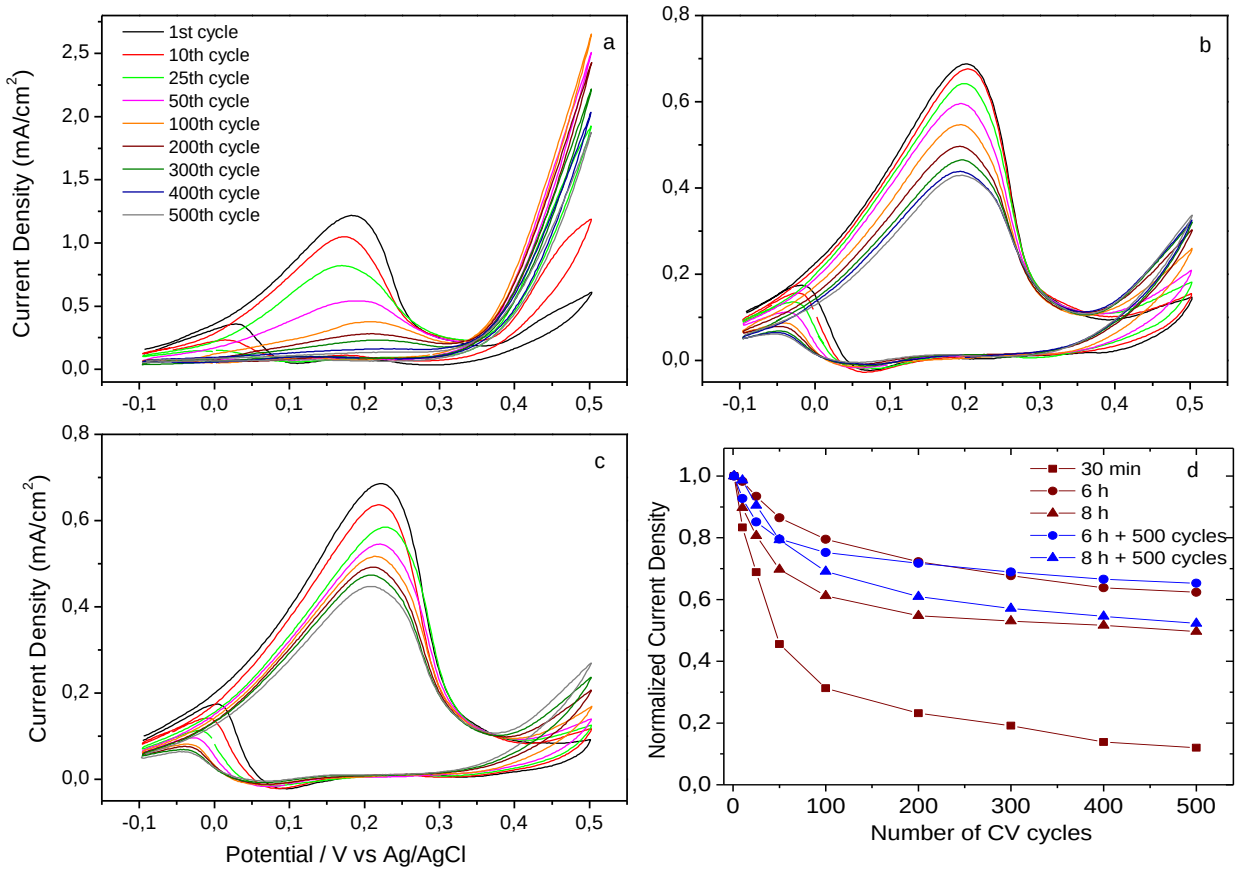
a
1st cycle
10th cycle
25th cycle
50th cycle
100th cycle
200th cycle
300th cycle
400th cycle
500th cycle
Current Density (mA/cm2)
b
c
Current Density (mA/cm2)
Potential / V vs Ag/AgCl
d
30 min
6 h
8 h
6 h + 500 cycles
8 h + 500 cycles
Normalized Current Density
Number of CV cycles